ARMY RESEARCH LABORATORY

Urban Turbulence and Wind Gusts for Micro Air Vehicle Bio-inspired Designs

by Cheryl L. Klipp and Edward Measure

ARL-TR-5492   **March 2011**

NOTICES

Disclaimers

The findings in this report are not to be construed as an official Department of the Army position unless so designated by other authorized documents.

Citation of manufacturer's or trade names does not constitute an official endorsement or approval of the use thereof.

Destroy this report when it is no longer needed. Do not return it to the originator.

Army Research Laboratory

Adelphi, MD 20783-1197

ARL-TR-5492   **March 2011**

Urban Turbulence and Wind Gusts for Micro Air Vehicle Bio-inspired Designs

Cheryl L. Klipp and Edward Measure
Computational and Information Sciences Directorate, ARL

REPORT DOCUMENTATION PAGE

1. REPORT DATE *(DD-MM-YYYY)*	2. REPORT TYPE	3. DATES COVERED (From - To)
March 2011	DRI	

4. TITLE AND SUBTITLE	5a. CONTRACT NUMBER
Urban Turbulence and Wind Gusts for Micro Air Vehicle Bio-inspired Designs	
	5b. GRANT NUMBER
	5c. PROGRAM ELEMENT NUMBER

6. AUTHOR(S)	5d. PROJECT NUMBER
Cheryl L. Klipp and Edward Measure	FY 10CIS-07
	5e. TASK NUMBER
	5f. WORK UNIT NUMBER

7. PERFORMING ORGANIZATION NAME(S) AND ADDRESS(ES)	8. PERFORMING ORGANIZATION REPORT NUMBER
U.S. Army Research Laboratory ATTN: RDRL-CIE-D 2800 Powder Mill Road Adelphi, MD 20783-1197	ARL-TR-5492

9. SPONSORING/MONITORING AGENCY NAME(S) AND ADDRESS(ES)	10. SPONSOR/MONITOR'S ACRONYM(S)
	11. SPONSOR/MONITOR'S REPORT NUMBER(S)

12. DISTRIBUTION/AVAILABILITY STATEMENT

Approved for public release; distribution unlimited.

13. SUPPLEMENTARY NOTES

14. ABSTRACT

We discuss the effects of wind turbulence encountered in an urban street canyon on very small unmanned aerial vehicles (UAVs) in the context of field data from the Joint Urban 2003 Experiment in Oklahoma City, OK. We present equations for the aerodynamics of such a UAV and derive equations to estimate the torque and forces encountered as a function of turbulent changes in wind velocity. We use sonic anemometer data from the experiment to compute wind velocity changes over a daylong sampling period with a temporal resolution of one tenth of a second. These changes are then used to compute resulting forces on notional UAVs of size comparable to small birds and butterflies, and for a Wasp II UAV for comparison. Computations are made for three locations using data measured near the middle of the street canyon at 1.5 and 15.7 m above ground level (AGL), as well as at 8.0 m AGL in a nearby intersection. We show graphs of turbulent kinetic energy, maximum acceleration encountered, and others. We found that accelerations greater than one gravity occur frequently, especially for the lighter vehicles, and accelerations of several gravities were common.

15. SUBJECT TERMS

Micro UAV, urban turbulence

16. SECURITY CLASSIFICATION OF:			17. LIMITATION OF ABSTRACT	18. NUMBER OF PAGES	19a. NAME OF RESPONSIBLE PERSON Cheryl L. Klipp
a. REPORT	b. ABSTRACT	c. THIS PAGE	UU	28	19b. TELEPHONE NUMBER *(Include area code)*
Unclassified	Unclassified	Unclassified			(301) 394-2543

Contents

List of Figures

INTENTIONALLY LEFT BLANK.

1. Objective

The objective of this effort is to develop a more realistic understanding of turbulence effects on small aircraft to aid in the design of these small vehicles, improve computer modeling of small scale turbulence, and ultimately produce effective decision aids for the deployment of small aircraft in urban settings.

2. Approach

2.1 Properties of Turbulence

Turbulence is a property of the flow, not the fluid. It is heavily influenced by boundary conditions. There is no official definition of turbulence. Most modern textbooks just list some of the properties of turbulent flow (Kundu, 1990; Shivamoggi, 1998) such as the following:

- Large fluctuations about the mean values

- Enhanced rates of momentum, heat and mass transport

- Multiple scales of motion

- Without energy input, the turbulent motion decays

Although turbulence data can be approximated (figure 1) with a Gaussian probability density function (pdf), in reality, there are "fat tails" with slightly more extreme values than predicted by a Gaussian with the same mean and standard deviation (figure 2a). Even more important than the slight variation from Gaussian statistics is the fact that the data are not organized in a random manner, at least not over short time and spatial scales (Frisch, 1995). The differences between closely spaced (in time or space) adjacent data points, which are important to determining the instantaneous forces on micro flyers, do not have a Gaussian pdf (figure 2b). Turbulent data is not random data but has some kind of organization. Due to the small size of the new micro unmanned aerial vehicles (UAVs), this organization becomes more significant than it would be for a larger aircraft.

Gaussian based spectral models to simulate the wind fluctuation fields are the best option available to micro-system developers. These models do not capture the non-Gaussian wind difference. The ability to completely simulate all properties of turbulent wind fields is a current topic of research. Rosales and Meneveau (2006) have been able to replicate non-Gaussian wind differences while maintaining spectral and other properties, but fully admit that their method fails to replicate vortical structures. To remedy this shortcoming of computer simulated data, this

report uses measured field data. Such data can provide a useful supplement and corrective to the known deficiencies of the simulations.
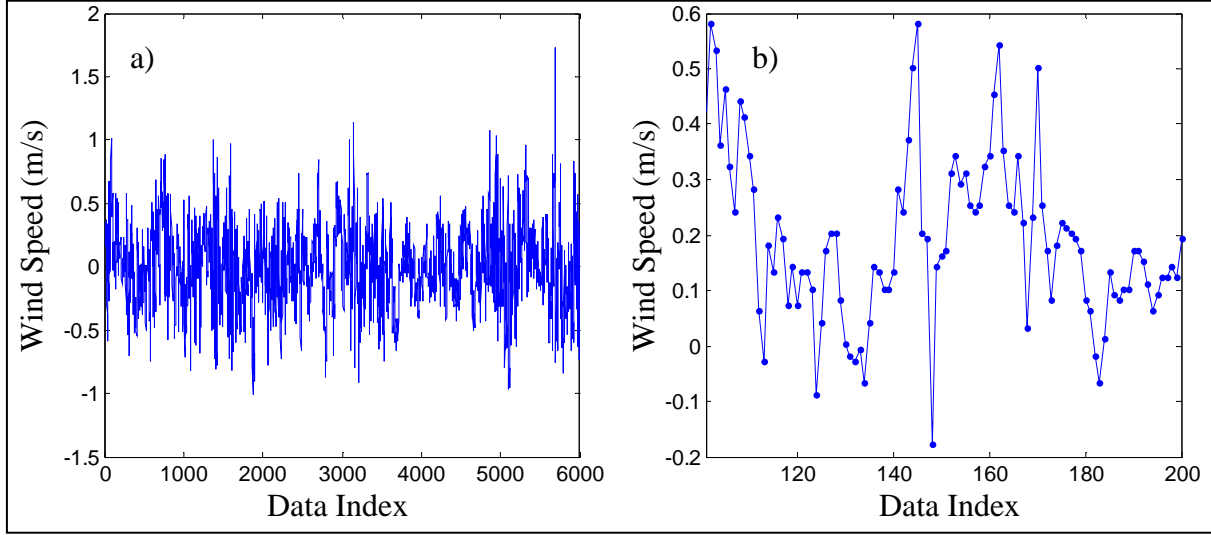
Figure 1. (a) Ten minutes of vertical component data, 1800–1810 universal time coordinated (UTC) (near noon local time) of day 190, and (b) 10 s of the same data.
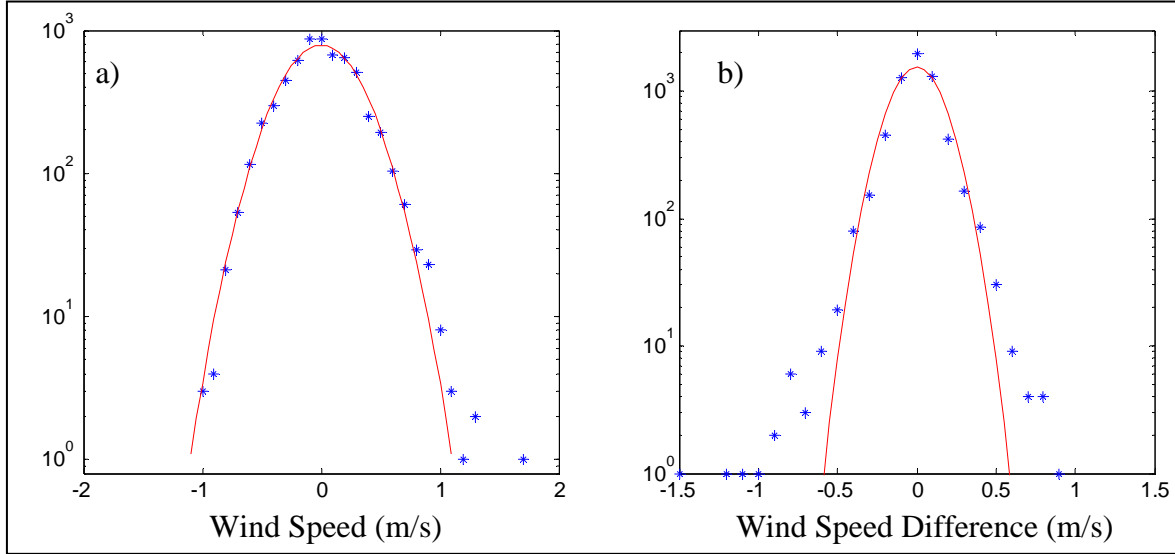
Figure 2. (a) PDF of 10 min of vertical component data in figure 1, 1800–1810 UTC (the red line is Gaussian with same mean and standard deviation as data), and (b) pdf of differences between adjacent data points.

2.2   Turbulence and the Micro UAV

The micro UAV is more vulnerable to turbulence than its bigger cousins for both dynamic and environmental reasons. Dynamically, its smaller size and lower speed means that much smaller forces can significantly affect its trajectory. Environmentally, it is more vulnerable because it is expected to fly in the highly cluttered, turbulent atmosphere near the ground. Maneuvering in a

turbulent atmosphere cluttered with potential obstacles is thus a daunting task, but it is one that birds, bats, and insects routinely solve, and solve using only onboard sensors and remarkably slow information processing systems—processors with a cycle time one million times slower than that of a modern microprocessor.

Turbulent structure on a scale comparable to its own size can yaw, pitch, and (especially) roll the aircraft. For a characteristic aircraft dimension of l, these tumbling forces scale like l^2 (wing area, for example), the resultant torques scale like $l \times f \propto l^3$ but the moment of inertia I scales like $I \propto Mass \times l^2 \propto l^5$. Consequently, as size decreases, the tendency to tumble or slew increases quadratically.

Suppose that force ma corresponded to an uncompensated torque of $\tau = mab/5$, where b is the wingspan, and further assume that the relevant moment of inertia was $I = mb^2/10$ (compare a solid cylinder of diameter d at $md^2/8$). Then angular acceleration α is given by

$$\alpha = \tau/I = (mab/5)/(mb^2/10) = 2\,a/b. \tag{1}$$

So for a $b = 20$ cm wingspan and acceleration $a = G = 9.8$ m/s^2, $\alpha = 98$ radians/s^2, which if uncompensated for 0.1 s leads to a roll of 28°.

Turbulent variations in wind speed and direction also result in changes in the lift force. A resulting linear acceleration of 1G uncompensated for 0.1 s produces a displacement of 4.9 cm. The displacement becomes 4.9 m if the acceleration is uncompensated for a full second. Even the smaller number could threaten a vehicle attempting to move through tight spaces. At the realistically encountered acceleration of 3G, a 5.0-cm displacement occurs in less than 60 ms. In sections 2.3–2.5, we have adopted a threshold of a 1G (9.8 m s^{-2}) acceleration for the designation of "significant events."

2.3 Lift Equation

The fundamental equation of lift (Tennekes, 2009) is

$$L = \frac{1}{2}C_L \rho A v^2 , \tag{2}$$

where L is lift, C_L is the lift coefficient, ρ is air density, A is wing area, and v is the airspeed. The lift coefficient C_L is a complicated function of wing shape and angle of attack, but for a thin wing at small angles of attack

$$C_L \cong 2\pi\theta , \tag{3}$$

where θ is the angle of attack (in radians). For most flyers, natural and manmade, the optimal angle of attack is on the order of 6° and the airspeed is adjusted so that the total lift force balances the force of gravity.

2.4 Relative Impact of Turbulence in the Vertical and Horizontal

In a turbulent wind, the fluctuating components of the wind speed appear as fluctuations in the airspeed and angle of attack (steady winds affect the ground velocity but not the airspeed). The effect on lift can be summarized by

$$dL = \frac{1}{2}\rho A v^2 \left(\frac{\partial C_L}{\partial \theta}\right) d\theta + C_L \rho A v dv \tag{4}$$

with dv as the fluctuating component of the wind. For the small angle, thin wing approximation for the coefficient of lift

$$\frac{\partial C_L}{\partial \theta} \cong 2\pi . \tag{5}$$

For small angles, the angle between $\vec{v}$ and $\vec{v} + dv$ is

$$d\theta \cong \sin(\theta) = |(\vec{v} + dv) \times \vec{v}| / (|\vec{v} + dv \parallel \vec{v}|) . \tag{6}$$

Maximum values of $d\theta$ occur when the fluctuating component is perpendicular to the main component and

$$d\theta \cong |dv| / |\vec{v}| . \tag{7}$$

Maximum changes in the airspeed, by contrast, occur when the velocity fluctuation is parallel to the air speed. Let us compare the two terms for the rather benign case where air speed = 5 m/s and the fluctuating wind component is $dv = 0.2$ m/s. From the vertical component data in figure 1, this is seen to be reasonable. Then the maximum value of $d\theta = 0.04$.

A normal cruising speed value of the angle of attack is about 0.11 (in radians), so a fluctuation of that magnitude ($d\theta = 0.04$) in the perpendicular direction would represent a 36% fluctuation in lift, dL/L. For a parallel component of the same magnitude, we have the following:

$$\frac{dL}{L} = \left(\frac{2vdv}{v^2}\right) = \frac{2}{25} = 8\% . \tag{8}$$

The modest turbulence in our example is enough to drastically affect the trajectory of the aircraft. The 36% lift change cited, for example, would produce a significant velocity change.

Such errors are much too large for remotely controlled flight through a complicated airspace of trees, branches, and window openings. It is quite clear that autonomous real-time sensing and control are needed for such maneuvers.

The fundamental physics of flight dictates that an aircraft support itself against gravity by transferring downward momentum to air at a rate $dp/dt = mg$. At cruising speed V, and optimal angle of attack, wing area A and lift L (and consequently aircraft weight mg) are related approximately as

$$L = mg = 0.4 \, V^2 A. \tag{9}$$

For flapping flight, this requires adjustment for the fact that lift takes place only on the down stroke and also for unsteady aerodynamic effects, which permit higher angles of attack and consequently smaller wings (Sane, 2003). Analyses in the current report are confined to fixed-wing craft, but the effects of turbulence are similar when the above differences are allowed for. The more complex aspects of flapping flight, and its advantages for small flyers, are deferred to later work.

2.5   Setup of Wind Field

To calculate the effects of turbulence on a small aircraft, we first need to set up a turbulent wind field for the aircraft to traverse. Wind field simulator software algorithms are very sophisticated but are fundamentally stochastic, whereas turbulent data over short distances/small time scales are not stochastic (Frisch, 1995). So instead of using a simulated wind field, we use a constructed wind field using data taken from a street canyon and intersection in Oklahoma City, OK, as part of the Joint Urban 2003 (JU2003) Defense Threat Reduction Agency (DTRA) and Department of Homeland Security (DHS) funded field campaign (Allwine and Flaherty, 2006). The data are the three components of the wind vector measured at a rate of 10 times per second with sonic anemometers deployed at a variety of locations within the Park Avenue street canyon (see the appendix for details of the sonic anemometer).

The day of year 190, corresponding to 9 July 2003, was chosen for its fairly typical and steady properties. Upwind of the urban center, 30 m above ground level, the mean wind speed for the day was 6.6 m/s, with slightly slower winds at night, slightly faster during the day. The mean wind direction was 192° ± 10°. This is roughly at right angles to the east-west oriented Park Avenue street canyon axis, but winds in the canyon were channeled along the canyon axis. For this day sunrise was at 11:20 UTC, solar noon at 18:35 UTC, and sunset at 1:50 UTC (from the National Oceanic and Atmospheric Administration (NOAA) online solar calculator).

The three-dimensional wind vector data from a fixed anemometer are used to establish a spatially distributed wind field through the application of Taylor's frozen turbulence hypothesis (Frisch, 1995; Kaimal and Finnigan, 1994), which makes the assumption that the turbulent part of the wind field is evolving at a sufficiently slow rate compared to the mean wind speed that one can visualize the turbulent wind field as being frozen as it is advected past the anemometer by the mean wind velocity.

The dots in figure 3 represent the location of "frozen turbulence" data points moving with the wind. The points are irregularly spaced due to turbulent variability in wind speed, U_X. The time

5

between points is fixed, in this case at 0.1 s, so the spacing between adjacent points, i and $i{-}1$, is the mean wind speed between the two points multiplied by 0.1 s: $\Delta x_i = (u_{xi} + u_{xi-1}/2)\Delta t$. Typical scales for Δx_i are 10–20 cm at mid-canyon and 20–40 cm in the intersection. These are comparable to the scale of small aircraft. When the aircraft traverses this field at its optimal airspeed, U_F, the spatial scales translate into temporal scales of 7–35 ms at the mid-canyon location and 13–52 ms in the intersection. Human remote control is unlikely to be able to react quickly enough to compensate for turbulence.
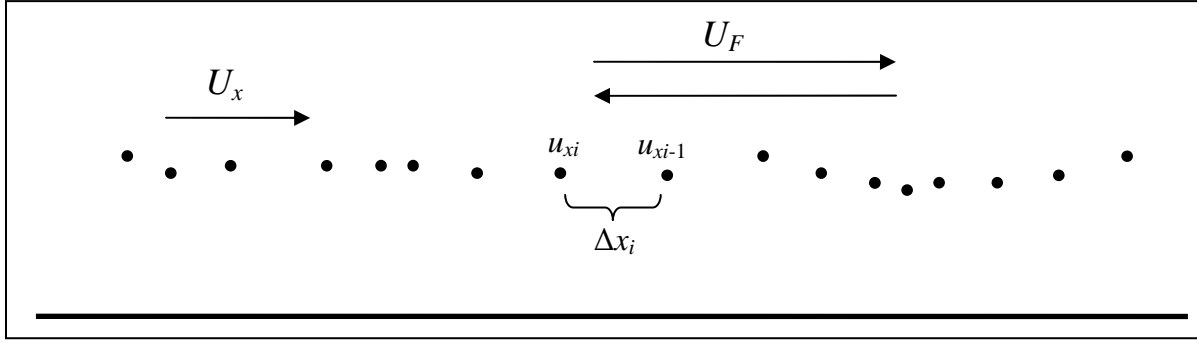
Figure 3. The locations of frozen turbulence data points being advected by the mean wind, U_X. Aircraft will then traverse the data fields at an optimal mean wind speed U_F.

The data at each point is the deviation at that point from the mean vertical and along-canyon wind vector components. This is added to the optimal airspeed vector U_F to create the wind field. The combination of airspeed and mean wind speed make up the ground speed of the aircraft. Since the details of how quickly an aircraft can react to and recover from turbulence induced changes in lift will vary with the engineering details of each aircraft, we have made the simplifying assumption that steady level flight is attained between each wind field point.

The resulting wind field data at each point are plugged into the lift equation, equations 2 and 3, to obtain a lift force at each data point. Assuming that steady level flight was attained at the previous point, the difference in lift from one point to the next is the net force on the aircraft between the two data points. With $F = (L_i - L_{i-1})$, the acceleration is $a = F/m$, where m is the mass of the aircraft. For most of this analysis the mass used is 3 g and a wing area of 12 cm^2, comparable to a hummingbird as well as some of the small aircraft under development. It is assumed that the aircraft is flying parallel to the canyon axis. Secondary mean flows and turbulence in the cross-canyon direction are not accounted for.

3. Results

Turbulence kinetic energy (TKE) is a common measure of the strength of turbulence. Figure 4 shows time series of TKE for the three locations analyzed in this report, 1.5 and 15.7 m above street level at a mid-canyon location 8 m from the south side of the canyon, and at 8.0 m above

street level at the southeast corner of the intersection to the east of the canyon. As is typical of the atmosphere, daytime turbulence levels are higher than nighttime levels (local noon is at 1830 UTC). Also typical of urban turbulence, levels of TKE are higher in the intersections than inside the urban canyon (Nelson et al., 2007; Ramamurthy et al., 2007; Roth, 2000; Grimmond et al., 1998; Rotach, 1995).
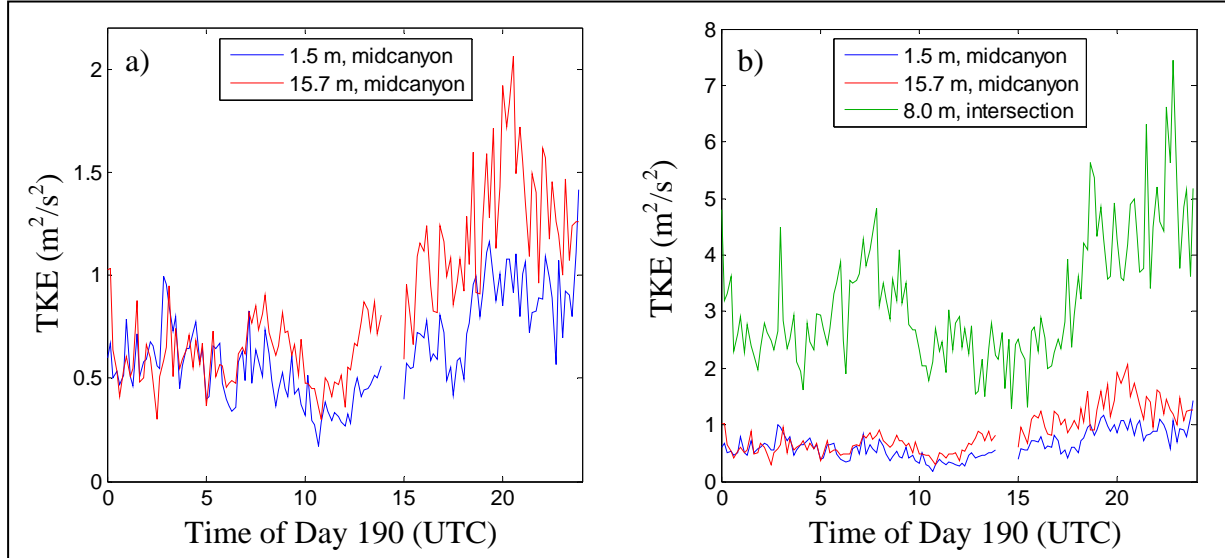
Figure 4. (a) Time series of TKE in each 10-min block of data at the mid-canyon tower. Note that the TKE levels are lower at night than in the day, also that TKE levels are comparable at the two levels at night, but the higher elevation has greater TKE levels in the day compared to TKE levels at the lower elevation. (b) Is the same as (a) but with intersection data added. TKE levels in the intersection are considerably larger than at the mid-canyon location.

As discussed in section 2.2, a threshold acceleration of 1G was chosen as a metric to categorize the effects of turbulence on small aircraft. Figure 5 is the time series of the number of times the acceleration exceeded 1G in each 10-min block of data. At night, the lower elevation sonic, 1.5 m, encounters more high G accelerations than the upper level sonic, 15.7 m. During the day, the situation is reversed. It is not yet known if this is true in general or just for this case. As might be expected, times and locations with higher TKE levels encounter significant events more often than lower TKE times. The intersection has a much higher number of high G accelerations than any of the mid-canyon levels. These events are calculated using a hummingbird mass to wing area ratio.
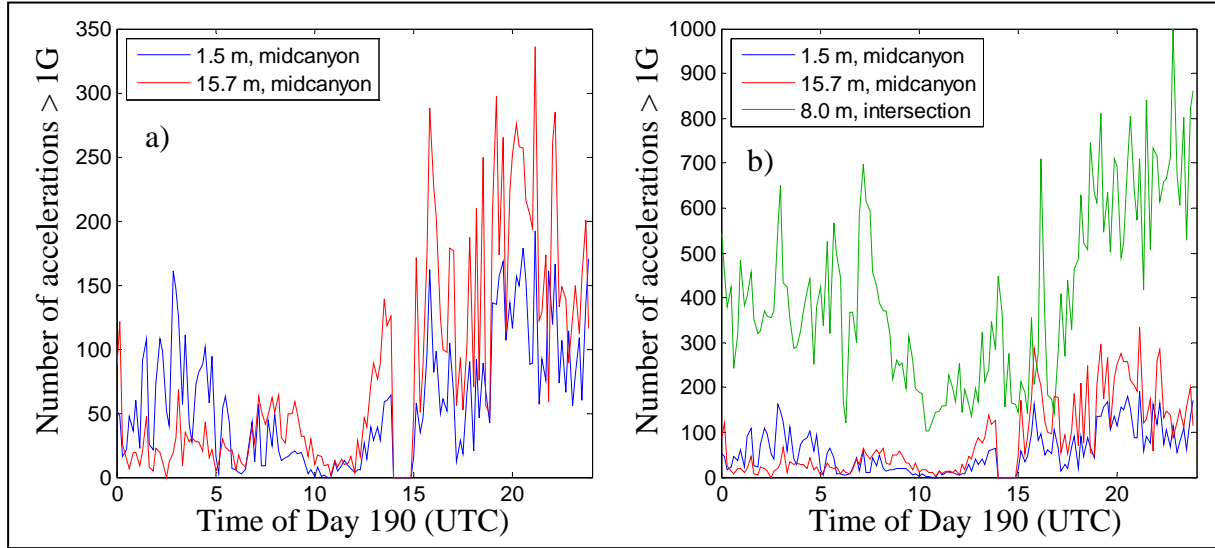
Figure 5. (a) Time series of number of accelerations greater than 1G in each 10-min block of data at the mid-canyon tower (6000 data points). At night, the lower level has more high G accelerations than the upper level. During the day, the situation is reversed. (b) Is the same as (a) but with intersection data added. The intersection has a much higher number of high G accelerations than any of the mid-canyon levels. All are calculated for the hummingbird mass/area ratio.

Another useful metric to determine effects of turbulence on small aircraft is the maximum acceleration encountered in a block of time (10 min) plotted in figure 6. The TKE–maximum acceleration correlation is less clear than the correlation between TKE and fraction of significant events. Although the intersection location encounters larger maximum values than the canyon location, the difference is not as large as might be expected based solely on TKE values (figure 4b). The largest mid-canyon acceleration occurs at the 1.5-m elevation at night, and even in the daytime, larger accelerations can occur at the lower elevation, also an indication that TKE is not the only factor.
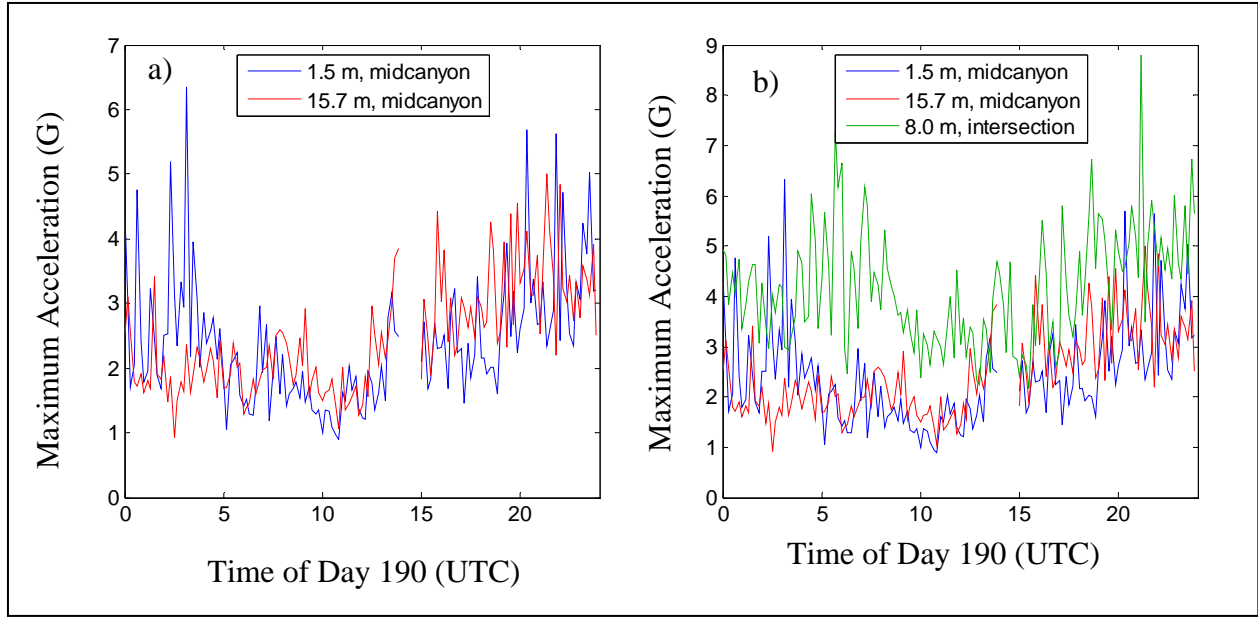
Figure 6. (a) Time series of maximum acceleration in each 10-min block of data at the mid-canyon tower. Note that the largest mid-canyon acceleration occurs at the 1.5 m level at night, and even in the daytime, larger accelerations occur at the lower level. (b) Is the same as (a) but with intersection data added. The intersection usually has higher accelerations than mid-canyon, with a few exceptions at night. All are calculated for the hummingbird mass/area ratio.

The scatter plots in figure 7 of the maximum acceleration in a 10-min block as a function of the number of significant events in the same block show that the number of greater than 1G events in a 10-min block is not a good predictor of the maximum acceleration in that block. Comparing the number of significant events to the TKE in each block of data shows that TKE is a fairly good predictor of the number of accelerations greater than 1G (figure 8), while plots of the maximum acceleration as a function of TKE show that TKE is a poor predictor of the maximum acceleration (figure 9).
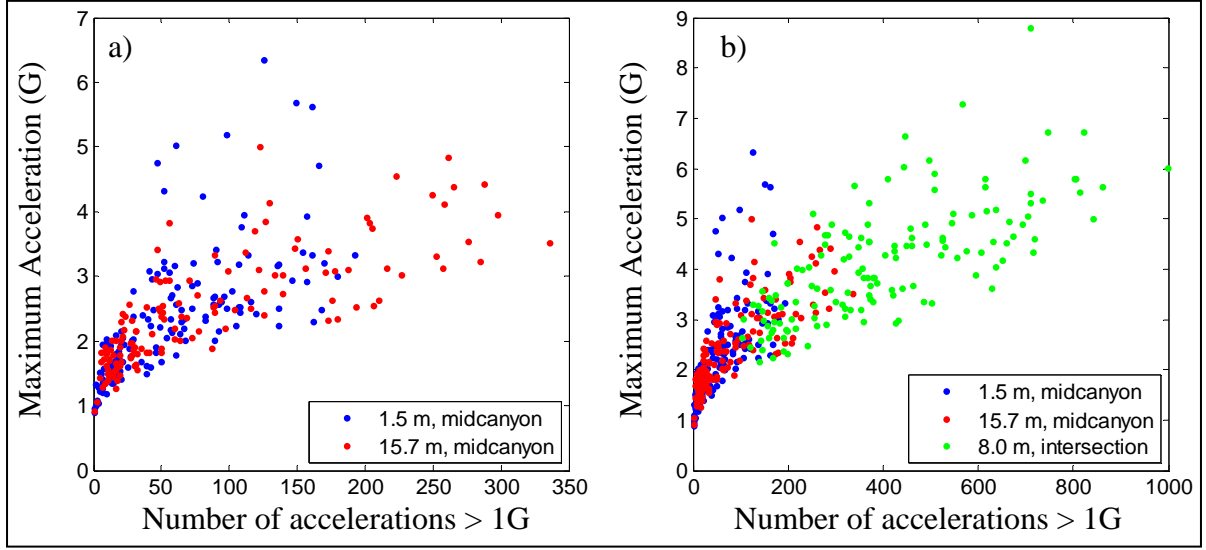
Figure 7. (a) Maximum acceleration as a function of the number of accelerations greater than 1G in each 10-min block of data at the mid-canyon tower. Note that the largest mid-canyon acceleration does not correspond to the largest number of greater than 1G events. Also note that accelerations of 2G occur even when the number of greater than 1G events is relatively low. (b) Is the same as (a) but with intersection data added. All are calculated for the hummingbird mass/area ratio.
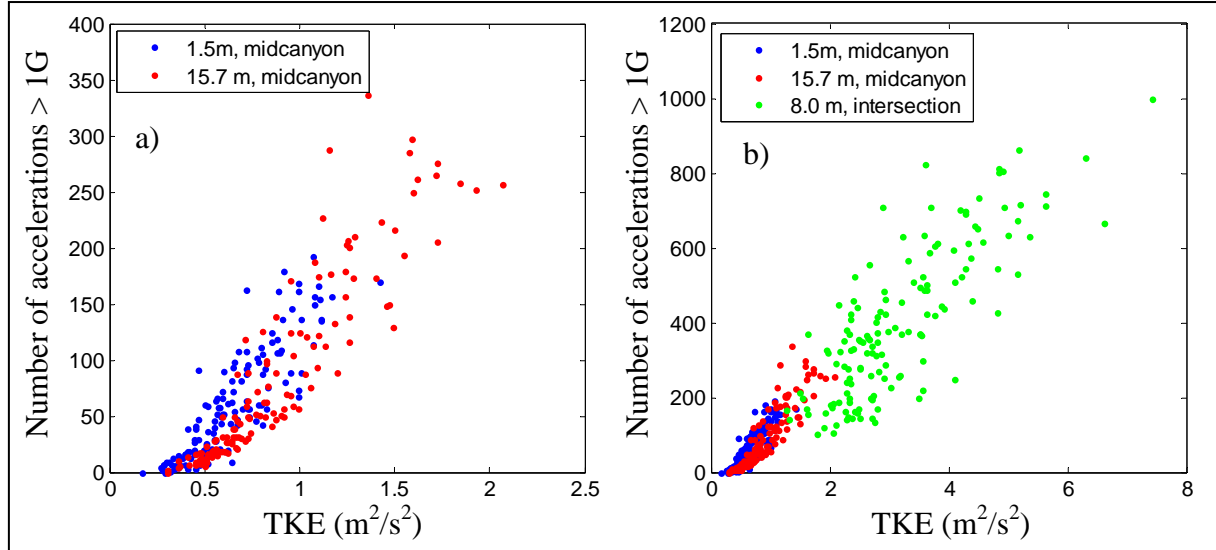
Figure 8. (a) Number of accelerations greater than 1G in each 10-min block of data at the mid-canyon tower (6000 data points) as a function of TKE for a humming bird mass/area ratio. TKE is a reasonable predictor of the number of accelerations greater than 1G. (b) Is the same as (a) but with intersection data added.
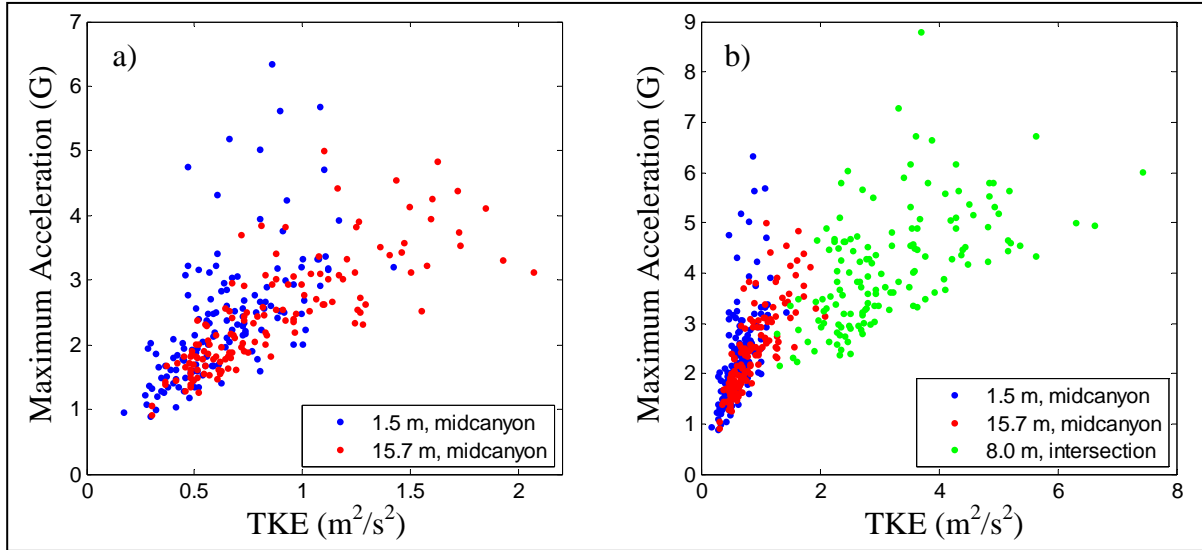
Figure 9. (a) Maximum acceleration in each 10-min block of data at the mid-canyon tower as a function of TKE for a humming bird mass/area ratio. Note that TKE is not a good predictor of maximum acceleration. (b) Is the same as (a) but with intersection data added.

Given equations 2, 3, and 9, the ratio of mass to wing area determines the accelerations generated by the wind data. This ratio is also called wing loading. The hummingbird and wren have similar ratios and therefore have similar accelerations (figure 10). The butterfly, having a small mass and relatively large wing area, feels the impact of the turbulence as a significantly larger number of significant events. The results for the mass to wing area ratio of the fielded WASP II UAV are shown for comparison, however, its physical size is too large for this analysis to be realistic. The wing loading is about 2.5 kg/m^2 for a hummingbird, 2.2 kg/m^2 for a wren, 0.2 kg/m^2 for a butterfly, and 6.0 kg/m^2 for the WASP II UAV. For comparison, the wing loading for many commercial airliners is in the range of 650–800 kg/m^2.
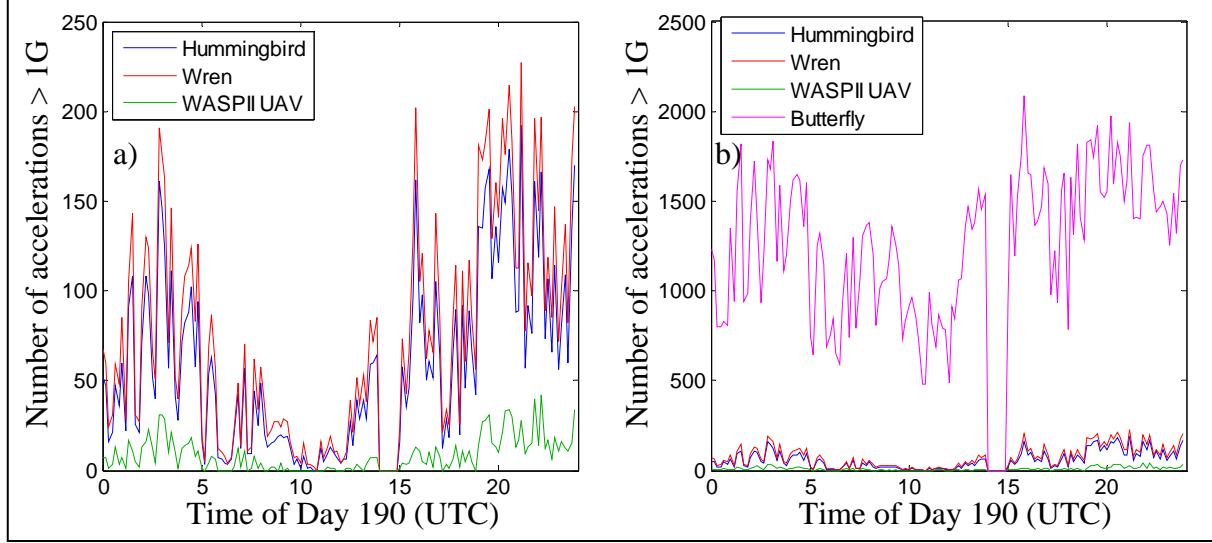
Figure 10. (a) Number of accelerations greater than 1G in each 10-min block of data (6000 data points) at the 1.5 m level of the mid-canyon tower for different aircraft types. Humming birds and wrens have similar mass/area ratios and therefore similar responses to turbulence. The possible response of the WASP II UAV is included for reference. (b) is the same as (a) but with butterfly data added. The much smaller mass/area ratio makes butterflies more susceptible to turbulence.

4. Conclusions

This work used actual measured urban turbulence data to compute resultant accelerations of several small aircraft with a simplified model of flight dynamics. The analysis carried out in this effort has several limitations that suggest the desirability of a more complete and detailed analysis. Our data set, though one of the most extensive in existence, samples just one city during one month and has no high wind events, strongly hinting that far more severe effects are likely. Also, because the data set was taken at 10 samples per second, smaller scale turbulent events are not resolvable, with the smallest measurable structures in this data set being rather larger than the smallest UAV. Finally, the concentration of our analysis on the number of events exceeding our threshold of 1G acceleration and the maximum acceleration provides only two metrics for effects that ultimately need full aerodynamic simulations to characterize.

Several compelling findings have come out of this analysis, in spite of its limitations. One is that turbulence intermittency is significant at scales on the order of tens of centimeters in urban turbulence. Some schools of thought consider turbulence intermittency to be significant only at scales comparable to or smaller than the Kolmogorov dissipation scale, which is on the order of millimeters for atmospheric flows. Given the 10-cm transducer separation and the data rate of 10 per second, translating to spatial rates of tens of centimeters, the data from these sonic anemometers are too coarse to show dissipation scale phenomena, and therefore not expected to

resolve intermittency phenomena. These sonics are able to resolve inertial scales that start at about 1 Hz in the atmosphere and extend beyond the Nyquist frequency (5 Hz for the data used here). Some researchers have found intermittency to be observable at inertial scales, but intermittency at inertial scales is inconsistent with Kolmogorov turbulence theory, making intermittency at inertial scales unpalatable.

Another significant finding is that the primary influence of turbulence at this scale is in changes in the angle of attack in the lift equation rather than the speeding up or slowing down of the wind in the direction of flight. Since it is possible that the nature of turbulent fluctuations above the atmospheric boundary layer are quite different than the street level turbulence studied here, it is not known if these findings scale up to commercial air traffic.

Another conclusion is that human remote control is unable to react quickly enough to the effects of turbulence. This makes it necessary for turbulence control to be onboard and autonomous whether or not overall flight control is remote or autonomous.

Also unique to this work is the manner in which field data are used as a turbulent wind field for modeling effects on aircraft. Typically, computer simulated turbulence fields are used by the design community. Since the computer generated fields do not reproduce intermittency, we have devised a manner in which field data can be used instead. This method produces more realistic wind fields than the simulated fields, but to obtain the more closely spaced data more appropriate for nano-UAVs, an instrument other than a sonic anemometer will be needed.

5. References

Allwine, K. J.; Flaherty, J. E. *Joint Urban 2003: Study Overview and Instrument Locations*; PNNL-15967; Pacific Northwest National Laboratory: Richland, WA, 2006.

Frisch, U. *Turbulence: The Legacy of A. N. Kolmogorov*, Cambridge University Press: New York, NY, **1995**, pp. 296.

Grimmond, C.S.B.; King, T. S.; Roth, M.; Oke, T. R. Aerodynamic Roughness of Urban Areas Derived from Wind Observations. *Boundary-Layer Met.* **1998**, *98*, 1–24.

Heinemann, Detlev; Langner, Dirk; Stabe, Ulf; Waldi, Hans-Peter. Measurement and correction of ultrasonic anemometer errors and impact on turbulence measurements, 1997 http://www.energiemeteorologie.de/publications/wind/conference/1997/Measurement_and_ Correction_of_Ultrasonic_Anemometer_Errors_and_impact_on_turbulence_measurements.p df (accessed March 2011).

Kaimal, J. C.; Finnigan, J. J. *Atmospheric Boundary Layer Flows*, Oxford University Press, **1994**, pp. 289.

Kundu, P. K. *Fluid Mechanics*, Academic Press, Inc.: San Diego, CA, **1990**, pp. 638.

Nelson, M. A.; Pardyjak, E. R.; Klewicki, J. C.; Pol, S. U.; Brown, M. J. Properties of the Wind Field Within the Oklahoma City Park Avenue Street Canyon, Part I: Mean Flow and Turbulence statistics. *J. of Applied Meteorology and Climatology* **2007**, *46*, 2038–2054.

Ramamurthy, P.; Pardyjak, E. R.; Klewicki, J. C. Observations of the Effects of Atmospheric Stability on Turbulence Statistics Deep Within an Urban Street Canyon. *J. of Applied Meteorology and Climatology* **2007**, *46*, 2074–2085.

Rosales, C.; Meneveau, C. A Minimal Multiscale Lagrangian Map Approach to Synthesize Non-Gaussian Turbulent Vector Fields. *Physics of Fluids* **2006**, *18*, 075104

Rotach, M. W. Profiles of Turbulence Statistics In and Above an Urban Street Canyon. *Atmospheric Environment* **1995**, *29*, 1473–1486.

Roth, M. Review of Atmospheric Turbulence Over Cities. *Q. J. R. Meteorol. Soc.* **2000**, *126*, 941–990.

Sane, Sanjay P. The Aerodynamics of Insect Flight. *J. of Experimental Biology* **2006**, *206*, 4191–4208.

Shivamoggi, B. K. *Theoretical Fluid Dynamics*, 2nd ed.; John Wiley and Sons: NewYork, NY, **1998**, pp. 555.

Tennekes, H. *The Simple Science of Flight: From Insects to Jumbo Jets*, rev. ed., MIT Press, **2009**, pp. 176.

6. Transitions

This work will transition into the U.S. Army Research Laboratory (ARL) program for biologically inspired approaches to environmental awareness and control of small unmanned aerial systems (UASs) in turban environments. In conjunction with this Director's Research Initiative (DRI), we delivered some preliminary results to Dr. J. Sean Humbert, Assistant Professor at University of Maryland and director of the Autonomous Vehicle Laboratory, to inform his group of the non-Gaussian nature of turbulent fluctuations as they might impact their robotic micro flyer design program. The present work will be of interest to Professor Inderjit Chopra and several graduate students from the University of Maryland's Department of Aerospace Engineering as well. The present full report will be forwarded as a follow-up to those previous interactions. In addition, the work performed here will be of interest to micro flyer designers and those who are planning for the future use of micro sensors on micro flyers for urban surveillance missions inside and outside of buildings. Furthermore, Dr. Klipp will get in contact with Mr. Mark Bundy of the Vehicle Test Directorate (VTD) in the design and setup of a micro flyer test facility being put together by VTD near Aberdeen Proving Ground (APG), MD, to discuss characterization of turbulence in their test facility using a sonic anemometer to help confirm future work. Dr. Measure will discuss the work with his SBIR Phase II contractors developing biomimetic navigation for small and micro UAV.

Follow-on research should address inclusion of the cross wind turbulence component and secondary higher order fluctuation effects to complete the picture of time dependent forces on micro flyers in urban domains.

INTENTIONALLY LEFT BLANK.

Appendix. Sonic Anemometer: Principle of Operation

Sound waves in air are carried with the wind, so that a sound wave going downwind covers ground faster than one headed in the opposite direction. That fact forms the basis for the operation of the sonic (or ultrasonic) anemometers that were used for the measurements discussed here. Sonic anemometers usually have paired transducers that transmit sound pulses forward and back, measuring the travel time in each case.

Kaimal and Finnigan (1994) discuss the principle of operation of the sonic anemometer and thermometer in their book *Atmospheric Boundary Layer Flows* (pp. 247–249). Much of the discussion below is adapted from theirs, and from Heinemann et al. (1997).

If A and B are transducers located a distance d apart, and the component of wind in the direction from A to B is v, then the transit time from A to B is

$$t_{AB} = d/(c + V_d), \tag{A-1}$$

while the transit time in the opposite direction is

$$t_{BA} = d/(c - V_d), \tag{A-2}$$

where c is the speed of sound in air and V_d is the along path component of the wind velocity. The transit time measurements permit computation of V_d and c. We know c approximately, of course, but it does vary, being proportional to the square root of the virtual temperature, so the virtual temperature can also be inferred. In the ideal gas approximation, the equation for the velocity of sound in air is

$$c_{sound} = \sqrt{\frac{\gamma R T}{M}} \ , \tag{A-3}$$

where $\gamma \equiv C_p / C_v$ = the adiabatic constant; C_p and C_v are the specific heats at constant pressure and constant volume, respectively; R is the universal gas constant; T is absolute temperature; and M is the average molecular weight of the gas.

Consequently, T can be inferred from the speed of sound to be

$$T = M c_{sound}^2 / \gamma R. \tag{A-4}$$

Since the average molecular weight of air varies with humidity, it is usually more convenient to just use the molecular weight of dry air, M_{dry} in which case we get the virtual temperature T_v

$$T_v = M_{dry} c_{sound}^2 / \gamma R. \tag{A-5}$$

Typical sonic anemometers have either two or three mutually orthogonal such pairs of transducers permitting two- or three-dimensional measurements of the wind. All the data considered in this report were taken with three-dimensional sonic anemometers. Numerous effects combine to limit the precision, accuracy, and time resolution with which the winds can be measured, many of which are discussed in Kaimal and Finnigan (1994).

List of Symbols, Abbreviations, and Acronyms

APG	Aberdeen Proving Ground
ARL	U.S. Army Research Laboratory
DHS	Department of Homeland Security
DRI	Director's Research Initiative
DTRA	Defense Threat Reduction Agency
JU2003	Joint Urban 2003
NOAA	National Oceanic and Atmospheric Administration
Pdf	probability density function
TKE	turbulence kinetic energy
UAS	unmanned aerial system
UAVs	unmanned aerial vehicles
UTC	universal time coordinated
VTD	Vehicle Test Directorate

1   ADMNSTR
(PDF   DEFNS TECHL INFO CTR
ONLY)   ATTN DTIC OCP
          8725 JOHN J KINGMAN RD STE 0944
          FT BELVOIR VA 22060-6218

1 HC   US ARMY RSRCH LAB
          ATTN RDRL CIM G T LANDFRIED
          BLDG 4600
          ABERDEEN PROVING GROUND MD 21005-5066

3 HCS   US ARMY RSRCH LAB
          ATTN IMNE ALC HRR MAIL & RECORDS MGMT
          ATTN RDRL CIM L TECHL LIB
          ATTN RDRL CIM P TECHL PUB
          ADELPHI MD 20783-1197

3 HCS   US ARMY RSRCH LAB
1CD   ATTN RDRL CIE D C KLIPP (1 CD, 1 HC)
          ATTN RDRL CIE S CHIEF
          ATTN RDRL CIE S A WETMORE
          ADELPHI MD 20783-1197

3 HCS   US ARMY RSRCH LAB
          ATTN RDRL CIE BE DIVISION
          ADELPHI MD 20783-1197

3 HCS   US ARMY RSRCH LAB
1CD   ATTN RDRL CIE D E MEASURE (1 CD, 1 HC)
          ATTN RDRL CIE D D HOOCK
          ATTN RDRL CIE M D KNAPP
          WSMR NM 88002

1 HC   US ARMY RSRCH LAB
          RDRL-VTA C KRONINGER
          APG BLDG 1120A
          ABERDEEN PROVING GROUND MD 21005-5066

1 HC   US ARMY RSRCH LAB
          RDRL-SER-L B PIEKARSKI
          ADELPHI MD 20783-1197

1 HC   US ARMY RSRCH LAB
          RDRL-SER-L G SMITH
          ADELPHI MD 20783-1197

1 HC   US ARMY RSRCH LAB
          RDRL-SER-L R POLCAWICH
          ADELPHI MD 20783-1197

TOTAL: 20 (1 ELEC, 2 CDS, 17 HCS)